HgCdTe/Si Materials for Long Wavelength Infrared Detectors

S.M. JOHNSON,[1,4] A.A. BUELL,[1] M.F. VILELA,[1] J.M. PETERSON,[1] J.B. VARESI,[1] M.D. NEWTON,[1] G.M. VENZOR,[1] R.E. BORNFREUND,[1] W.A. RADFORD,[1] E.P.G. SMITH,[1] J.P. ROSBECK,[1] T.J. DE LYON,[2] J.E. JENSEN,[2] and V. NATHAN[3]

1.—Raytheon Vision Systems, Goleta, CA 93117. 2.—HRL Laboratories LLC, Malibu, CA 90265. 3.—Air Force Research Laboratory, AFRL/VSSS, Kirtland AFB, NM 87117. 4.—E-mail: sjohnson1@raytheon.com

The heteroepitaxial growth of HgCdTe on large-area Si substrates is an enabling technology leading to the production of low-cost, large-format infrared focal plane arrays (FPAs). This approach will allow HgCdTe FPA technology to be scaled beyond the limitations of bulk CdZnTe substrates. We have already achieved excellent mid-wavelength infrared (MWIR) and short wavelength infrared (SWIR) detector and FPA results using HgCdTe grown on 4-in. Si substrates using molecular beam epitaxy (MBE), and this work was focused on extending these results into the long wavelength infrared (LWIR) spectral regime. A series of nine p-on-n LWIR HgCdTe double-layer heterojunction (DLHJ) detector structures were grown on 4-in. Si substrates. The HgCdTe composition uniformity was very good over the entire 4-in. wafer with a typical maximum nonuniformity of 2.2% at the very edge of the wafer; run-to-run composition reproducibility, realized with real-time feedback control using spectroscopic ellipsometry, was also very good. Both secondary ion mass spectrometry (SIMS) and Hall-effect measurements showed well-behaved doping and majority carrier properties, respectively. Preliminary detector results were promising for this initial work and good broad-band spectral response was demonstrated; 61% quantum efficiency was measured, which is very good compared to a maximum allowed value of 70% for a non-antireflection-coated Si surface. The R_0A products for HgCdTe/Si detectors in the 9.6-μm and 12-μm cutoff range were at least one order of magnitude below typical results for detectors fabricated on bulk CdZnTe substrates. This lower performance was attributed to an elevated dislocation density, which is in the mid-10^6 cm^{-2} range. The dislocation density in HgCdTe/Si needs to be reduced to $<10^6$ cm^{-2} to make high-performance LWIR detectors, and multiple approaches are being tried across the infrared community to achieve this result because the technological payoff is significant.

Key words: HgCdTe, heteroepitaxy, infrared detectors, molecular beam epitaxy (MBE), HgCdTe/Si, long wavelength infrared (LWIR)

INTRODUCTION

The heteroepitaxial growth of HgCdTe on large-area Si substrates is an enabling technology leading to the production of low-cost, large-format infrared focal plane arrays (FPA). This approach will allow HgCdTe FPA technology to be scaled beyond the limitations of bulk CdZnTe substrates. The development of this technology has had a long history, beginning in the 1980s. Early work used epitaxial GaAs/Si wafers as a starting template to grow CdTe or CdZnTe buffer layers, primarily using metal-organic vapor-phase deposition (MOCVD) or molecular beam epitaxy (MBE). The HgCdTe detector structures were then grown on these alternative substrates using liquid phase epitaxy (LPE) to fabricate mid-wavelength infrared (MWIR)[1] and long wavelength infrared (LWIR)[2] FPAs. Most of the research efforts are now focused on

(Received Feb. 10, 2004; accepted Feb. 25, 2004)

using CdTe grown directly on Si substrates, after it was first demonstrated by MBE.[3,4] LWIR FPAs were also produced using LPE-grown HgCdTe on MBE-grown CdZnTe/Si alternative substrates,[5] but this work has been discontinued in favor of an all MBE approach. The status of HgCdTe grown on Si substrates by MBE was reviewed in 1999.[6]

MBE HgCdTe/Si technology has matured significantly in the last few years and has been used to demonstrate state-of-the-art, short wavelength infrared (SWIR) and MWIR FPAs using HgCdTe grown on 4-in. (211)Si substrates.[7–10] For this technology to be more widely used, it is important to extend these results into the LWIR regime to realize the same benefits of using large-area HgCdTe/Si wafers. Historically, limitations in the performance of LWIR HgCdTe detectors on Si substrates have been attributed to a high dislocation density in the heteroepitaxial HgCdTe[2,5] because dislocations are known to degrade the performance of LWIR HgCdTe detectors, particularly at low temperatures.[11] We observe that typical values for dislocation density in MWIR HgCdTe grown on CdTe/Si are in the mid-10^6 cm^{-2} range as determined from etch-pit density (EPD) measurements, and this is relatively consistent with work published by other researchers. While this value of EPD has little effect on our MWIR HgCdTe/Si detectors, it must be reduced to achieve high-performance LWIR detectors. By comparison, HgCdTe epitaxial layers grown by MBE or LPE on bulk CdZnTe have typical EPD values in the 10^4 to mid-10^5 cm^{-2} range where there is a negligible effect of dislocation density on detector performance.

The objectives of this current work were to grow our baseline p-on-n double-layer heterojunction (DLHJ) detector structure used earlier for 4-in. MWIR HgCdTe/Si but extend the cutoff wavelength into the 9–10-μm LWIR spectral region, evaluate the material properties, and obtain some preliminary detector-performance data. Material characterization techniques included composition uniformity determined from Fourier transform infrared (FTIR) transmission, carrier concentration and mobility determined from Hall effect measurements, and dopant concentrations determined from secondary ion mass spectroscopy (SIMS). Detector properties include current-voltage (I-V) characteristics, spectral response, and quantum efficiency. These results are discussed and compared with HgCdTe detectors fabricated on bulk CdZnTe substrates.

MATERIAL GROWTH AND CHARACTERIZATION

LWIR HgCdTe p-on-n DLHJ structures were grown on 4-in. (211)Si wafers in a Riber (Rueil-Malmaison, France) Epineat system using our baseline process described earlier.[7–9] The growth is initiated with approximately 1 μm of ZnTe to ensure a (211)B orientation and is followed with a 6–8-μm layer of CdTe, which helps to reduce the propagation of threading dislocations. To maintain a clean growth surface, these substrates were never removed from the MBE system prior to growth of HgCdTe. The CdTe is used as a buffer layer rather than CdZnTe because our earlier work with CdZnTe grown by either MOCVD or MBE showed that the material properties, such as x-ray rocking curve full-width at half-maximum (FWHM), degrade as Zn is added to form the ternary alloy.[2,5] This appears to be particular to CdZnTe grown by vapor-phase techniques because the properties of bulk-grown CdZnTe are superior to those of CdTe for the alloy range used for lattice matching to HgCdTe. Currently, MBE-grown CdSeTe is being explored as a potentially better material for buffer layers on Si substrates.[12,13]

HgCdTe p-on-n DLHJ structures were grown on these CdTe/ZnTe/Si substrates using In for n-type and As for p-type doping. The composition profile was actively controlled using spectroscopic ellipsometry (SE) to determine the surface composition in real time and to feed back this information to adjust source fluxes.[9] A total of nine DLHJ HgCdTe/Si structures were grown sequentially.

The x = [CdTe] composition uniformity of the LWIR $Hg_{1-x}Cd_xTe$ absorber layer was determined from room-temperature FTIR transmission measurements that were made radially from the center-to-edge of the wafer in 5-mm steps. Figure 1 shows the composition at the center of the wafer as a function of run number and shows that the run-to-run composition control is very reproducible. The SE feedback control was lost during run 6, which is why that composition is significantly different from the others. Figure 2 shows the normalized composition (to the value at the center of the wafer) as a function of radial distance for a typical run (median value) obtained for this growth series. Figure 2 shows that the composition increases from center to edge, which was found earlier to be dependent on the effusion source configuration.[7] As a figure of merit for the 4-in. (100-mm) wafers, we have chosen the composition nonuniformity value measured at 45 mm, which represents the maximum nonuniformity and

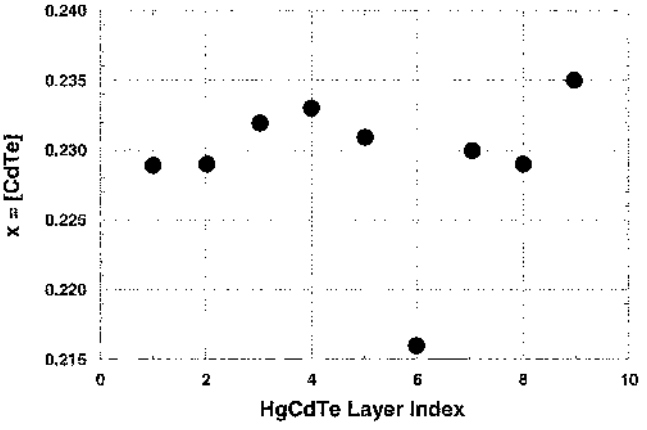

Fig. 1. The LWIR HgCdTe/Si composition at the center of the 4-in. wafer as a function of run number, which shows that the composition control is very reproducible.

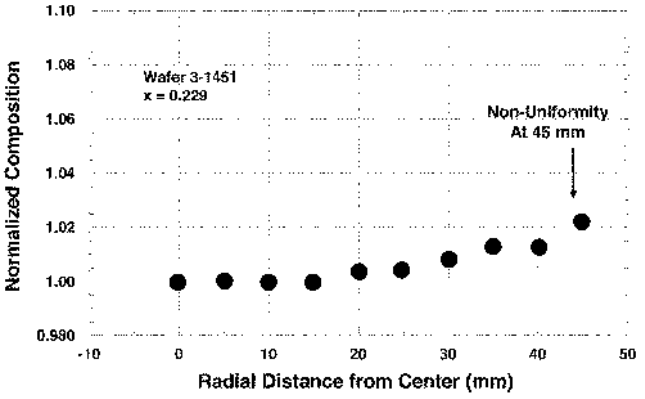

Fig. 2. Normalized LWIR HgCdTe/Si composition (to the value at the center of the wafer) as a function of radial distance for a typical growth run during this series.

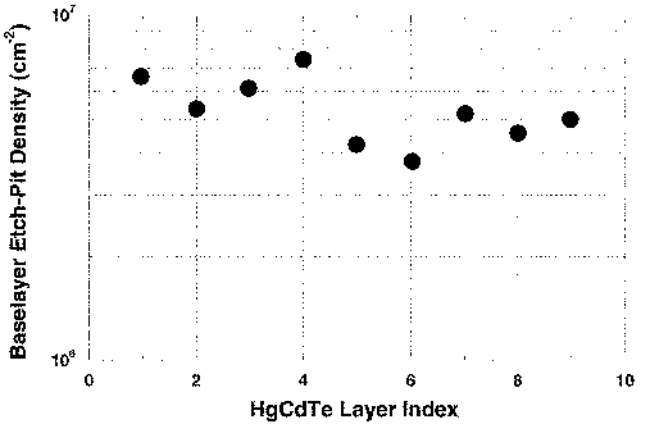

Fig. 4. Etch pit density in the LWIR HgCdTe/Si as a function of run number.

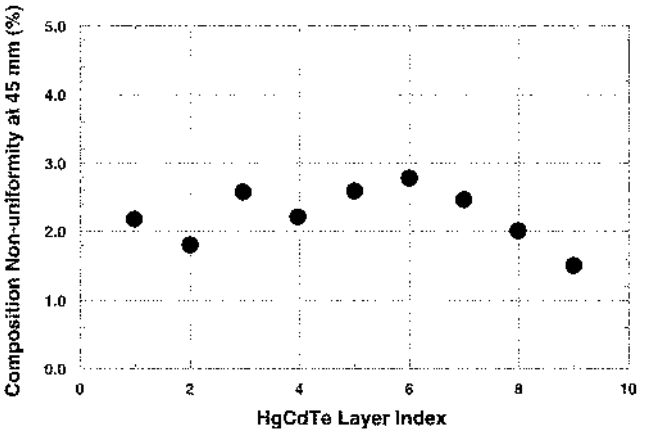

Fig. 3. LWIR HgCdTe/Si composition, nonuniformity value measured at 45 mm versus run number; this represents the maximum nonuniformity and is the closest point to the edge of the wafer that we can reliably make FTIR measurements.

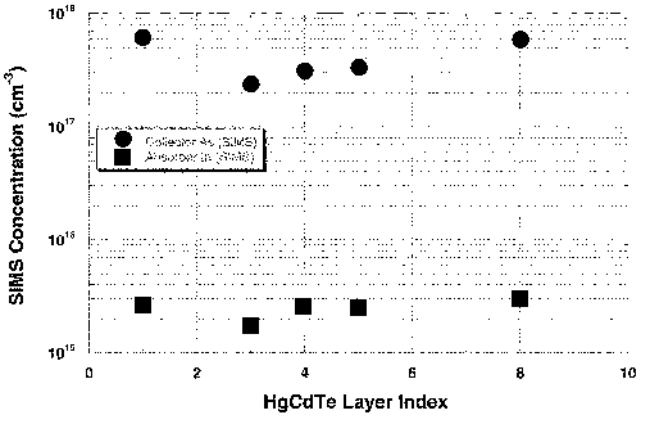

Fig. 5. [In] and [As] concentrations determined from SIMS measurements in the n-type absorber and p-type collector regions, respectively, showing that both of these doping concentrations are well-controlled and reproducible.

is the closest point to the edge of the wafer at which we can reliably make FTIR measurements. The wafer shown in Fig. 2 has a value 1.022 at 45 mm or a nonuniformity of 2.2%. Because the composition varies systematically with radius, this metric is a better representation of the nonuniformity than, for example, the standard deviation/mean (σ/mean). The wafer in Fig. 2 has a composition σ/mean = 0.74%, which is certainly lower but would be somewhat misleading. Figure 3 shows that the composition nonuniformity at 45 mm varies from 1.5–2.8% over this series of growth runs, which is reasonably low and repeatable for growth of LWIR HgCdTe over this large of a wafer.

Figure 4 shows a plot of the EPD in the LWIR HgCdTe as a function of run number. This figure shows that the EPD ranges from about 4–7 $\times$ 10^6 cm^{-2}, which is also very representative of those same values observed in our MWIR HgCdTe/Si materials. The [In] and [As] concentrations in the n-type absorber and p-type collector regions, respectively, were determined from SIMS measurements on five of the nine samples, as shown in Fig. 5. Figure 5 shows that both of these doping concentrations are well-controlled and reproducible from run to run.

Hall effect samples were prepared from all the wafers to determine the majority carrier properties of the n-type material. The p-type collector layer was etched off and van der Pauw samples were reticulated in a cloverleaf design. The samples were then annealed under Hg overpressure to fill residual Hg vacancies, and Hall effect measurements were made at room temperature, 77 K (LN_2), and 30 K (liquid neon) at a fixed magnetic field of 2.5 kG. Figure 6 shows a composite plot of the 77-K and 30-K mobilities and the 77-K carrier concentration versus run number. The mobility data in Fig. 6 is very consistent from run to run and increases to over 10^5 cm^2/V-s at 30 K, which is expected for LWIR HgCdTe material. The n-type, 77-K carrier concentration in Fig. 6 varies between 2–4 $\times$ 10^{15} cm^{-3} as expected from the SIMS measurements of the In-dopant concentration.

DETECTOR PERFORMANCE

Several of the wafers were selected for detector processing using our standard, HgCdTe DLHJ processing techniques consisting of mesa-etched diodes

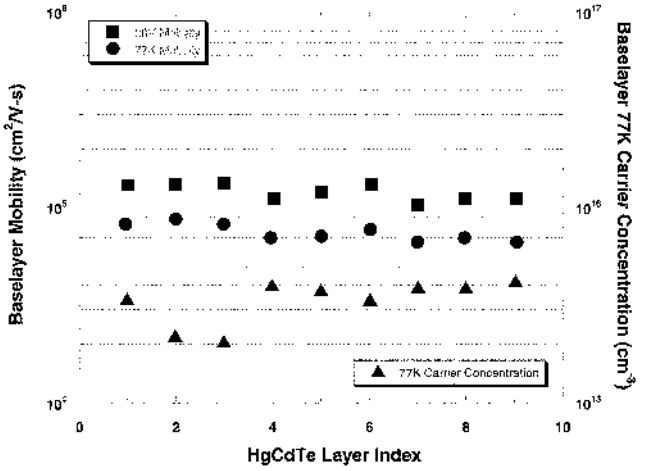

Fig. 6. Composite plot of the 77K and 30K mobilities and the 77K carrier concentration versus HgCdTe/Si run number determined from Hall effect measurements; these properties are well-behaved and have values expected for LWIR HgCdTe.

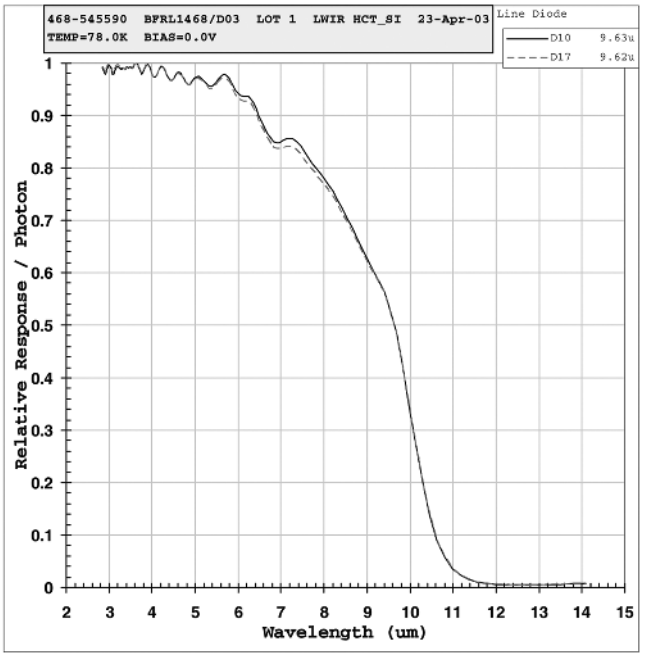

Fig. 7. Relative spectral response per photon versus wavelength for two 60-μm diodes in a mini-array having a cutoff of 9.6 μm; the cutoff is 10 μm if spectral response per watt is used. The quantum efficiency measured at 6.53 μm is 61%.

that are passivated with CdTe. Test structures consisting of variable-area and mini-array diodes were characterized using I-V characteristics, spectral response, and quantum efficiency measurements at 78 K. Figure 7 is a plot of the relative spectral response per photon versus wavelength for two 60-μm diodes in a mini-array showing a cutoff of 9.6 μm; the cutoff is 10 μm if spectral response per watt is used. Figure 7 shows that spectral response is relatively flat at short wavelengths, indicating good carrier collection within the LWIR absorbing region. The shape of the spectral response at longer wavelengths can be sharpened by increasing the absorber

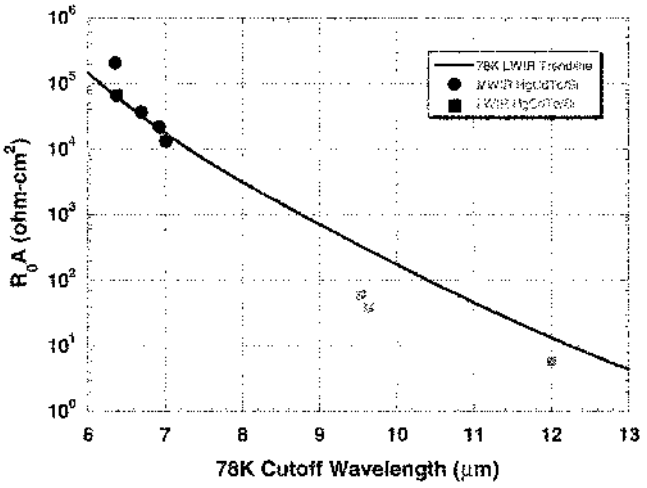

Fig. 8. Trendline of the median R_0A values versus cutoff wavelength (per photon) for various HgCdTe/Si mini-array diodes at 78K.

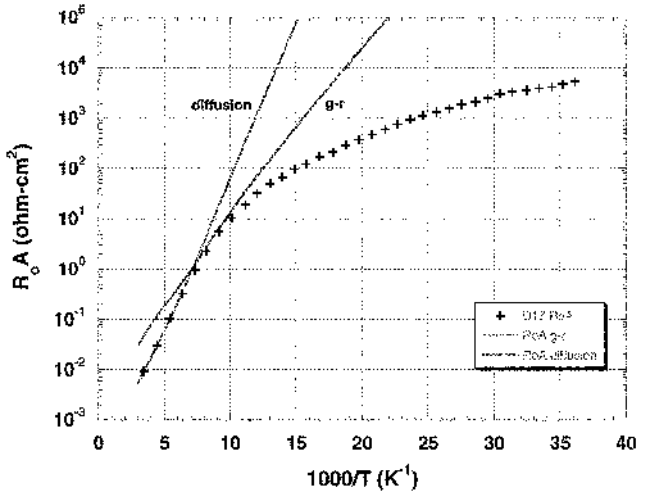

Fig. 9. The R_0A product versus inverse temperature for one of the mini-array diodes having a 78K cutoff of 9.6 μm.

layer thickness because for this baseline experiment, it was kept the same as that of our MWIR detectors. The quantum efficiency of these detectors was measured using a spike filter at 6.53 μm and was 61%, which is very good because there is a 30% reflectance loss from the bare Si backside-illuminated surface that limits the quantum efficiency to a maximum value of 70%. This quantum efficiency is easily increased using an antireflection coating on this surface.

Figure 8 displays a trendline of the median R_0A values versus cutoff wavelength (per photon) for various mini-array diodes at 78 K. The data in the 6–7-μm wavelength range are a few of the longest wavelength MWIR HgCdTe/Si arrays that we had tested earlier at 140 K[8–10] and were retested at 78 K. The curve labeled 78-K LWIR trendline is shown just to illustrate the trend expected for diffusion-limited detectors. The LWIR HgCdTe/Si detector results are at least one order of magnitude below that typically seen for HgCdTe grown on bulk CdZnTe.

To better understand the leakage current mechanisms in these detectors, I-V characteristics were measured as a function of temperature. Figure 9 shows a plot of R_0A versus inverse temperature for one of the mini-array diodes whose spectral response is shown in Fig. 7. At temperatures above approximately 140 K, the data follows the correct slope (varies as n_i^{-2}) for a diffusion-limited diode, but below this temperature, the data rapidly deviates from this slope. The slope for a generation-recombination-limited detector (varies as n_i^{-1}) is also shown in Fig. 9 but does not account for the shape of the experimental data at lower temperatures. The data in Fig. 9 is similar to that observed in HgCdTe p-on-n DLHJ detectors with high dislocation density.[11] Therefore, it is likely that the high dislocation density (mid-10^6 cm^{-2}) in these HgCdTe/Si detectors is responsible for the excess leakage. The dislocation density in HgCdTe/Si detectors needs to be reduced to $<10^6$ cm^{-2} to make high-performance LWIR detectors. The use of dislocation blocking layers, CdSeTe/Si substrates,[12,13] and thermal annealing[14] are all potential techniques that can be applied to reduce the threading dislocation density in the active detector region.

SUMMARY AND CONCLUSIONS

The heteroepitaxial growth of HgCdTe on large-area Si substrates is an enabling technology leading to the production of low-cost, large-format infrared FPAs. This approach will allow HgCdTe FPA technology to be scaled beyond the limitations of bulk CdZnTe substrates. We have already achieved excellent MWIR and SWIR detector and FPA results using HgCdTe grown on 4-in. Si substrates using MBE, and this work was focused on extending these results into the LWIR spectral regime. A series of nine, p-on-n, LWIR HgCdTe, DLHJ detector structures were grown on 4-in. Si substrates. The HgCdTe composition uniformity was very good over the entire 4-in. wafer, with a typical maximum nonuniformity of 2.2% at the very edge of the wafer; run-to-run composition reproducibility, realized with real-time feedback control using SE, was also very good. Both SIMS and Hall effect measurements showed well-behaved doping and majority carrier properties, respectively. Preliminary detector results were promising for this initial work, and good broad-band spectral response was demonstrated; 61% quantum efficiency was measured, which is very good compared to a maximum allowed value of 70% for a non-antireflection-coated Si surface. The R_0A products for HgCdTe/Si detectors in the 9.6-μm and 12-μm cutoff range were at least one order of magnitude below typical results for detectors fabricated on bulk CdZnTe substrates. This lower performance was attributed to an elevated dislocation density, which is in the mid-10^6 cm^{-2} range. The dislocation density in HgCdTe/Si needs to be reduced to $<10^6$ cm^{-2} to make high-performance LWIR detectors, and multiple approaches are being tried across the infrared community to achieve this result because the technological payoff is significant.

ACKNOWLEDGEMENTS

This work was sponsored by MDA, monitored by AFRL Contract No. F29601-02-C-0298, and also supported by Raytheon IR&D. The authors gratefully acknowledge the support of all of these organizations.

REFERENCES

1. S.M. Johnson, M.H. Kalisher, W.L. Ahlgren, J.B. James, and C.A. Cockrum, *Appl. Phys. Lett.* 56, 946 (1990).
2. S.M. Johnson et al., *J. Electron. Mater.* 22, 835 (1993).
3. Y. Lo, R.N. Bicknell, T.H. Myers, J.F. Schetzina, and H.H. Stadelmaier, *J. Appl. Phys.* 54, 4238 (1983).
4. R. Sporken, S. Sivananthan, K.K. Mahavadi, G. Monfroy, M. Boukerche, and J.P. Faurie, *Appl. Phys. Lett.* 55, 1879 (1989).
5. S.M. Johnson, T.J. de Lyon, C.A. Cockrum, W.J. Hamilton, T. Tung, F.I. Gesswein, B.A. Baumgratz, L.M. Ruzicka, O.K. Wu, and J.A. Roth, *J. Electron. Mater.* 24, 467 (1995).
6. T.J. deLyon, J.E. Jensen, M.D. Gorwitz, C.A. Cockrum, S.M. Johnson, and G.M. Venzor, *J. Electron. Mater.* 28, 705 (1999).
7. K.D. Maranowski, J.M. Peterson, S.M. Johnson, J.B. Varesi, W.A. Radford, A.C. Childs, R.E. Bornfreund, and A.A. Buell, *J. Electron. Mater.* 30, 619 (2001).
8. J.B. Varesi, R.E. Bornfreund, A.C. Childs, W.A. Radford, K.D. Maranowski, J.M. Peterson, S.M. Johnson, L.M. Giegerich, T.J. de Lyon, and J.E. Jensen, *J. Electron. Mater.* 30, 566 (2001).
9. J.B. Varesi, A.A. Buell, R.E. Bornfreund, W.A. Radford, J.M. Peterson, K.D. Maranowski, S.M. Johnson, and D.F. King, *J. Electron. Mater.* 31, 815 (2002).
10. J.B. Varesi, A.A. Buell, J.M. Peterson, R.E. Bornfreund, M.F. Vilela, W.A. Radford, S.M. Johnson, and D.F. King, *J. Electron. Mater.* 32, 661 (2003).
11. S.M. Johnson, D.R. Rhiger, J.P. Rosbeck, J.M. Petersen, S.M. Taylor, and M.E. Boyd, *J. Vac. Sci. Technol. B* 10, 1499 (1992).
12. Y. Chen, G. Brill, and N. Dhar, *J. Cryst. Growth* 252, 270 (2003).
13. Y. Chen, G. Brill, and N. Dhar, *J. Electron. Mater.* 32, 723 (2003).
14. M. Carmody et al., in this issue.